Observation of nonlinear dispersion relation and spatial statistics of wave turbulence on the surface of a fluid

Eric Herbert, Nicolas Mordant, Eric Falcon

Observation of nonlinear dispersion relation and spatial statistics of wave turbulence on the surface of a fluid

Eric Herbert,[1] Nicolas Mordant,[2] and Eric Falcon[1,*]

[1] *Matière et Systèmes Complexes (MSC), Université Paris Diderot, CNRS (UMR 7057) 10 rue A. Domon et L. Duquet, 75 013 Paris, France*

[2] *Laboratoire de Physique Statistique, École Normale Supérieure, CNRS, 24, rue Lhomond, 75 005 Paris, France*

(Dated: May 11, 2010)

We report experiments on gravity-capillary wave turbulence on the surface of a fluid. The wave amplitudes are measured simultaneously in time and space using an optical method. The full space-time power spectrum shows that the wave energy is localized on several branches in the wave-vector-frequency space. The number of branches depend on the power injected within the waves. The measurement of the nonlinear dispersion relation is found to be well described by a law suggesting that the energy transfer mechanisms involved in wave turbulence are not only restricted to purely resonant interaction between nonlinear waves. The power-law scaling of the spatial spectrum and the probability distribution of the wave amplitudes at a given wave number are also measured and compared to the theoretical predictions.

PACS numbers: 47.35.-i,05.45.-a,47.52.+j

Wave turbulence concerns the study of the statistical and dynamical properties of a set of numerous nonlinear interacting waves. It is an ubiquitous phenomenon observed in various situations from spin waves in solids, internal or surface waves in oceanography up to plasma waves in astrophysics (for recent reviews see [1, 2]). Wave turbulence theory, also called weak turbulence, predicts a wave energy cascade through the scales that can be derived analytically in nearly all fields of physics involving weakly nonlinear interacting waves in infinite systems [3]. However, few well-controled laboratory experiments have been performed so far, and show partial agreement with the theory [1, 2]. While most *in situ* or laboratory measurements involve time signals at a fixed location, theoretical predictions often concern the Fourier space. An important challenge is thus to get a space-time measurement of the turbulent wave amplitudes (as recently achieved for elastic wave turbulence [4]), and thus to have a better understanding of the elementary dynamical processes involved in the energy cascade. In the case of the wave turbulence on a fluid, 2D measurements are scarce and are achieved in oceanography by airbone remote sensing [5]. In laboratory, 1D [6, 7] or 2D [8] spatial measurements of the amplitude of gentle interacting waves exist. However, to our knowledge, no 2D spatial measurement has been performed for steep nonlinear waves as involved in wave turbulence.

Here, we investigate 2D spatial statistics of wave turbulence on the surface of a fluid. An optical method, based on Fourier transform profilometry [9, 10], provides the full space-time deformation field of the free-surface even when strongly nonlinear waves are involved. This leads to the first observation of the nonlinear dispersion relation. We also show that the energy transfer mechanisms during the cascade are not only restricted to purely resonant interactions between nonlinear waves as expected in weak turbulence [3], but also involve other mechanisms such as the formation of localized nonlinear structures (sharp-crested gravity waves) and of bound (or parasitic) gravity-capillary waves. Moreover, the scalings of the wave energy spectrum emphasize that the transition from k-space to ω-space cannot be done according to the linear wave dispersion relation as usually performed in wave turbulence experiments. Finally, the probability distribution of the Fourier mode amplitude is measured and shows a departure from the exponential at high Fourier wave amplitude.

The experimental setup consists of a rectangular tank, 46 cm $\times$ 36 cm in length, filled with water up to a depth of 7 cm. Surface waves are generated by the horizontal motion of two plunging rectangular Plexiglas wave makers (19 cm in width and 2 cm in depth). They are located at two corners of the same longest side of the tank, the vibration directions being perpendicular to each other [11]. The wave makers are driven by two electromagnetic shakers submitted to a random forcing within a narrow low-frequency band (typically from 1 to 4 Hz). When the forcing amplitude is increased, typical maximal crest-to-trough wave amplitude increases from 1 mm to 1.5 cm, whereas the wave mean steepness (ratio of crest-to-trough amplitude to its duration) increases from 0.2 up to 3.3 cm/s. This latter value corresponds to an injected power, P, 600 times greater than its value at the minimum forcing amplitude. This enables to access to linear, weakly and strongly nonlinear wave regimes. A Fourier transform profilometry method [9, 10] provides the temporal evolution of the vertical deformation of the free-surface of the fluid over a significant spatial zone of the tank. Namely, a fringe pattern (wavelength $\lambda_f = 2.6$ or 5.2 mm) is projected on the fluid surface by a video projector. When waves are generated, the vertical displacement of the free-surface leads to a phase shift of the

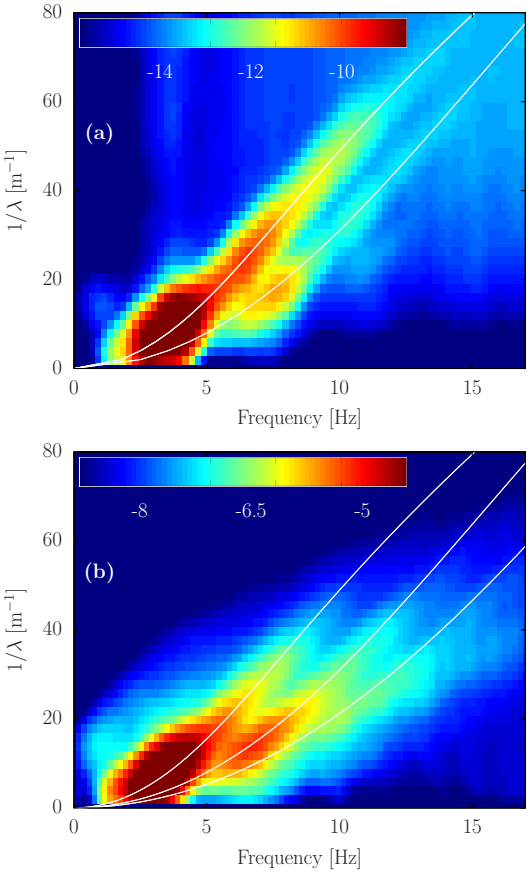

FIG. 1: (Color online) Space-time spectrum $E(k, f)$ of the vertical velocity of surface waves: moderate (a) and strong (b) injected powers [$P^{1/2} = 5.2$ (a) and 24.7 (b) in arb. units]. Forcing: 1 - 4 Hz. Colors are log scaled. Solid white lines are $\Omega_N(k)$ with $N = 1$, 2, and 3 (see text).

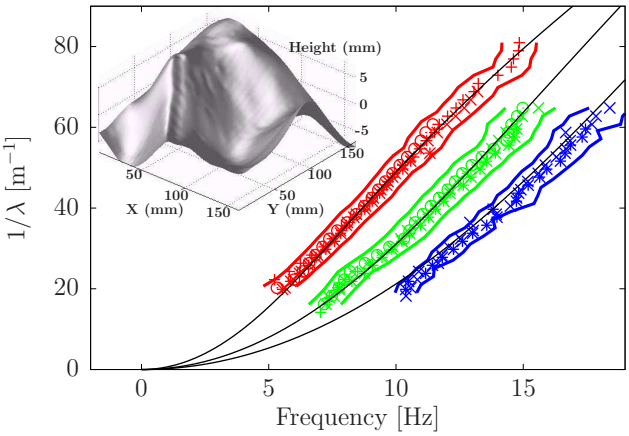

FIG. 2: (Color online) Nonlinear dispersion relation $k(f)$ computed from the lines of maximum energy of $E(k, f)$ for different forcings [$P^{1/2} = 1$ (+), 5.2, (○), 10.5 (×), 24.7 (∗)]. Solid thick lines around each branch correspond to the branch width averaged for all forcings. Solid lines are $\Omega_N(k)$ with $N = 1$, 2, and 3 (see text - same as in Fig. 1). Inset: snapshot of the wave amplitudes at strong forcing ($P^{1/2} = 24.7$).

pattern that is recorded by a high speed camera. The deformation of the fluid surface $\eta(x, y, t)$ is then recovered by a 2D phase demodulation of each image of the recorded movie [9, 10]. Movies are recorded with 1600 by 1200 pixels at $f_{acq} = 50$ or 60 Hz during roughly 1 minute. The size of the recorded image is $25 \times 19\,\mathrm{cm}^2$. To improve the contrast of the projected fringes on the fluid surface, a high concentrated white dye is added to the water bulk at an optimum concentration of 0.5% v/v [10]. The surface tension of this dyed water is measured to be $\gamma = 32 \pm 1\,\mathrm{mN/m}$. Spatial and temporal resolutions of the measurement are $3\lambda_f$ and $2/f_{acq}$.

The vertical velocity of the fluid surface $v(x, y, t)$ is obtained by differentiating the wave height movie in time. The full space-time power spectrum of the velocity $E(\mathbf{k}, f)$ (a function of both the wave vector $\mathbf{k}$ and the frequency f) is then computed from multidimensional Fourier transform. By integrating $E(\mathbf{k}, f)$ over all directions of $\mathbf{k}$, one obtains the velocity spectrum $E(k = ||\mathbf{k}||, f)$ displayed in Fig. 1 for moderate and strong forcings. We observe that the energy injected at low frequencies cascades through the scales and is mainly localized on several branches in the ($\omega \equiv 2\pi f$, $k \equiv 2\pi/\lambda$) space. At low forcing amplitude (not shown here), only one branch occurs that corresponds to the linear gravity-capillary relation dispersion $\omega(k) = \sqrt{gk + (\gamma/\rho)k^3}$, with $g = 9.81$ m/s^2 the acceleration of gravity, $\rho = 1000$ kg/m^3 the fluid density. When the forcing is increased (see Fig. 1a), a secondary branch appears below the linear dispersion relation. This branch is found to be well described by $\Omega_N(k) \equiv \sqrt{gNk + (\gamma/\rho)k^3/N}$ with $N = 2$ with no adjustable parameter (see solid line). At higher forcing (see Fig. 1b), a third branch appears below the second one that is also well governed by $\Omega_N(k)$ with $N = 3$. Thus, as the power injected in the wave system increases, the nonlinear wave interactions redistribute the wave energy on N branches govern by $\Omega_N(k)$, the nonlinear dispersion relation (NLDR). Since $\Omega_N(k) = N\omega_{k/N}$, at a fixed $k^\star$ corresponds N peaks ($\omega_{k^\star}$, $2\omega_{k^\star/2}$, $3\omega_{k^\star/3}$, $\cdots$) in a frequency Fourier spectrum, i.e. a horizontal slice of Fig. 1. This is consistent with a two-peak frequency spectrum reported in a numerical simulation [12].

At weak forcing, one observes linear gravity-capillary waves of gentle amplitudes that mix together. At strong forcing, steep long waves occur with sharp crest-ridges (see inset of Fig. 2). Near the crests of these waves, high order harmonics are generated: small gravity-capillary waves superimposed on the long wave are observed (see also [14]). These harmonics are called bound waves since they do not propagate with their own phase velocity but with the one of the carrier long wave [13], and thus leads to harmonics $\Omega_N(K)$ of velocity $\Omega_N(K)/K = \omega(k)/k$ where $K \equiv Nk$. They thus do not obey the linear dispersion relation which is consistent with the observation

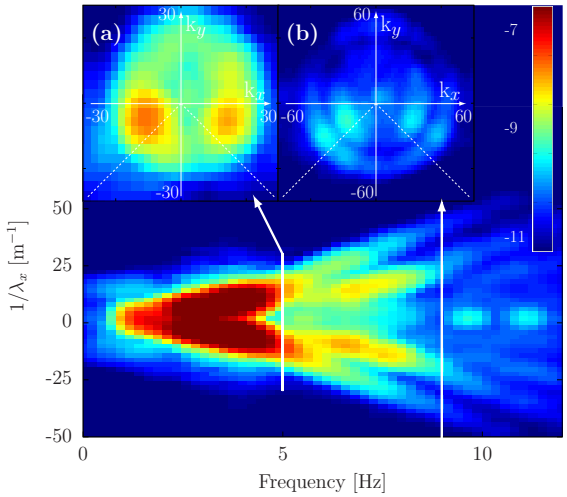

FIG. 3: (Color online) Space-time spectrum $E(k_x, f)$ of velocity at $P^{1/2} = 10.5$ located at $k_y = 0$. Same forcing bandwidth as in Fig. 1. Inset: space spectrum $E(k_x, k_y)$ located at f =5 Hz (a) and 9 Hz (b). Dashed lines: forcing directions. Log scaled colors are different for each plot.

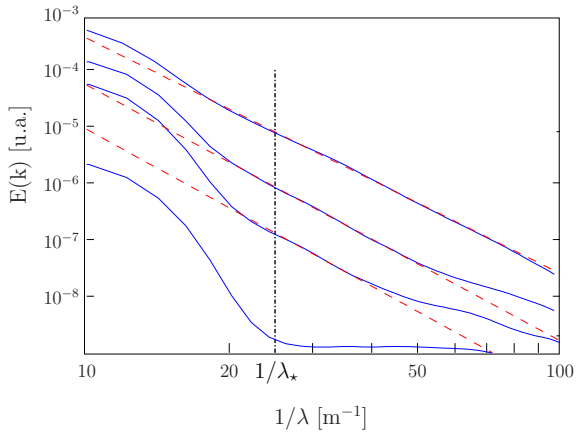

FIG. 4: (Color online) Spatial power spectrum $E(k)$ of the velocity for $P^{1/2}$ =1, 5.2, 10.5, 24.7 (from bottom to top). Dashed lines have slopes −4.6, −4.5 and −4.2 (from bottom to top). Dot-dashed line: $\lambda_\star^{-1} = 25.2\,\mathrm{m}^{-1}$ (see Fig. 5).

of secondary branches of the NLDR. This shows that other mechanisms than purely resonant wave interaction should be taken into account to describe the energy transfer across scales in wave turbulence.

Let us now focus on the effect of the injected power P on the location and the width of branches $\Omega_N(k)$. The maximum amplitude of each branch of the velocity spectrum $E(k, f)$ is extracted using the maximum of a Gaussian fit with respect to k at a fixed f. For different P, the lines of maximum energy of each branch are shown in Fig. 2 (symbols). Whatever the branch, the localized energy line is found to be independent of P: no measurable shift of these lines occurs in the (k,ω) space. This differs from recent observation reported in elastic wave turbulence [4] or in simulation [12]. The widths of these branches are also plotted in Fig. 2. The width is defined by the rms value of the Gaussian fit. Whatever the branch, no significant evolution of the width is found when P is increased. The width is also independent of the branch number within our experimental accuracy. The typical width [$\Delta(\lambda^{-1})$,Δf] centered on a point (λ^{-1},f) of the NLDR is roughly (8 m^{-1}, 1.5 Hz), and corresponds to a finite width of the non purely resonant interaction between waves. Thus, the wave energy is redistributed on different branches of the NLDR of width that is independent of P, and of the branch number.

Figure 3 shows different views of the full space-time Fourier spectrum of the velocity $E(\mathbf{k}, f)$. Main figure is $E(k_x, f)$, a slice at $k_y = 0$ of the spectrum along the x-axis. For frequencies above the forcing ones, one observes two branches in the positive k_x part and their symmetric in the negative part. This reveals the isotropy of the spectrum in both direction along the x-axis. Figures 3a and 3b then show $E(\mathbf{k})$ at two fixed frequencies (5 and 9 Hz). One distinguishes in Fig. 3b at least two concentric circles on the (k_x,k_y) plane corresponding to two wave numbers given by the above linear and nonlinear dispersion relation. Such circles show that the spectrum is roughly isotropic. Note that it is not fully isotropic since peaks of maximum amplitude are observed in both bottom quarters on each circle. These peaks are located on two axes corresponding to the ones of the wave generation by each wavemaker due to the forcing anisotropy (see Fig. 3). At a lower fixed frequency [see Fig. 3a], instead of different concentric circles corresponding to each branch, one rather observes a disc due to the overlapping of both branches of non-zero width (see above). Note also, here again, the presence of peaks in the two directions of the forcing. The spatial spectrum is thus found isotropic except in the vicinity and in the directions of the forcing.

The space spectrum $E(k \equiv ||\mathbf{k}||)$ of the velocity is then computed by summing the 3D space-time spectrum of $E(\mathbf{k}, f)$ over all the directions of $\mathbf{k}$ and over f. Figure 4 shows $E(k)$ when the forcing is increased. At high enough forcing, $E(k)$ is found to be scale invariant as expected for wave turbulence. The inertial range increases with the forcing, and $E(k) \sim k^{-n}$ with $n \simeq 4.2$ over almost one decade in k corresponding to $\lambda \sim$ few cm. Note that this exponent does not depend strongly on the forcing. Since one cannot compute $E(f)$ from $E(\mathbf{k}, f)$ in a wide range of frequencies due to the strong steepness of the spectrum, one performs single point temporal measurements that shows a strong dependence of the power-law frequency exponent of the velocity spectrum on the forcing as already reported (typically from f^{-5} to f^{-2}) [11, 15]. These scalings suggest that the change of variable $k \leftrightarrow f$ using the linear dispersion relation to estimate $E(k)$ from

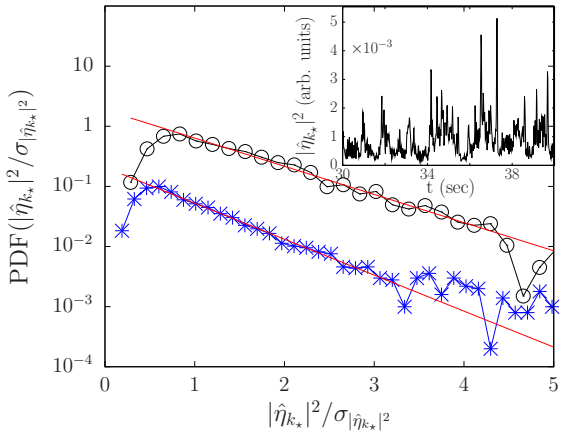

FIG. 5: (Color online) PDF of the Fourier wave amplitude, $|\hat{\eta}_{k_\star}|^2/\sigma_{|\hat{\eta}_{k_\star}|^2}$, at $k_\star \equiv 2\pi/\lambda_\star$ with $\lambda_\star^{-1} = 25.2 \pm 0.6\,\mathrm{m}^{-1}$ (see Fig. 4) for two forcings $P^{1/2} = 5.2$ (∘) and 10.5 (∗). $\langle|\hat{\eta}_{k_\star}|^2\rangle = 1.1$ (∘) and 1.3 (∗). Solid lines have slopes −0.46 and −0.58. Curves have been shifted vertically for clarity. Inset: $|\hat{\eta}_{k_\star}|^2$ vs. time. $\lambda_\star^{-1} = 25.2 \pm 0.6\,\mathrm{m}^{-1}$. $P^{1/2} = 24.7$.

$E(f)$ is not valid in temporal measurements in hydrodynamics wave turbulence when strong nonlinear waves are involved. Indeed, this would lead to an estimated velocity spectrum from k^{-3} to $k^{-3/2}$. Moreover, our scaling $E(k) \sim k^{-4.2}$ cannot be described by none of existing theories of wave turbulence taking into account either the presence of random-phased weakly nonlinear waves [$E_{theo}(k) \sim P^{1/2}k^{-1/2}$] [16] or the dominance of coherent sharp wave crests [$E_{theo}(k) \sim k^{-1}$ to k^{-3}] [7]. Since it is known numerically that the spatial spectrum exponent can change in case of anisotropy [17], one computes $E(k)$ by summing $E(\mathbf{k}, f)$ either over $k_y > 0$ where isotropy is checked or over $k_y < 0$ where anisotropy occurs due to the forcing reminiscence (see insets of Fig. 3). For the strongest forcing, the exponents found are 4.3 for $k_y > 0$ and 3.8 for $k_y < 0$ that is close to the previous 4.2 exponent. Our anisotropy thus not plays a significant role on the estimation of the spatial spectrum exponent.

Finally, we look at the probability density function (PDF) of the wave amplitude. First, the PDF of the wave amplitude $\eta(x, y)$ is found to be roughly Gaussian whatever the forcing. Second, one computes the PDF of the Fourier amplitude $|\hat{\eta}_{k_\star}|^2$ of a wave component at a given wave number $k_\star$. As shown in Fig. 4, we choose $k_\star \equiv 2\pi/\lambda_\star$ in the gravity regime with $\lambda_\star^{-1} = 25.2 \pm 0.6$ m^{-1} corresponding (using the linear dispersion relation) to a frequency of 6.5 Hz above the forcing ones. For each image, the value of $|\hat{\eta}_{k_\star}|^2$ is extracted by averaging on 42 amplitudes found on a $\mathbf{k}$-space ring of radius $k_\star$. Iterating for all images leads to the temporal evolution of the Fourier amplitude of the mode $k_\star$ as shown in Fig. 5. This signal is strongly erratic and bursts of random large-amplitude occurs. Similar random bursts of Fourier amplitude has been reported in numerical simulation [12], these bursts being correlated with phase jumps underlying strong nonlinear effects [12]. Although we are not able to measure the phase, this similarity is consistent with our above results underlying strong nonlinear effect. The PDF of the Fourier amplitude $|\hat{\eta}_{k_\star}|^2$, rescaled to its rms value $\sigma_{|\hat{\eta}_{k_\star}|^2}$, is then plotted in Fig. 5 for two forcings. At low forcing, the PDF is roughly exponential as expected for random and uncorrelated waves. At higher forcing, the PDF remains Gaussian up to three standard deviations, whereas its tail shows a slight departure from this Gaussian. Although more statistics are needed to characterize more deeply the PDF tail, this anomalously large probability of high Fourier mode amplitude is consistent with 1D spatial measurements [7], simulations [12] and theory [18].

In conclusion, we have reported 2D spatial statistics of wave turbulence on the surface of a fluid. The power spectrum, the nonlinear dispersion relation and the PDF of the Fourier modes show strong effects of nonlinear waves involved in wave turbulence. The spatial correlations and the role of the finite size of the basin should deserve more studies to have a complete description of the energy transfer mechanisms in wave turbulence.

This work has been supported by ANR Turbonde BLAN07-3-197846.

* E-mail: eric.falcon@univ-paris-diderot.fr

[1] E. Falcon, Discret. Contin. Dyn. Syst. B **13**, 819 (2010)
[2] A. Newell and B. Rumpf, *Wave Turbulence* submitted to Ann. Rev. Fluid Mech. (2010)
[3] V. E. Zakharov, G. Falkovich and V. S. L'vov, *Kolmogorov Spectra of Turbulence* (Springer–Verlag, 1992)
[4] P. Cobelli *et al.*, Phys. Rev. Lett. **103**, 204301 (2009)
[5] P. A. Hwang *et al.*, J. Phys. Oceanogr. **30**, 2753 (2000)
[6] D. Snouck, M.-T. Westra, and W. Van de Water, Phys. Fluids **21** 025102 (2009)
[7] S. Nazarenko, S. Lukaschuk, S. McLelland and P. Denissenko, J. Fluid Mech. **642**, 395 (2010)
[8] B. Jähne and K. S. Riemer, J. Geophys. Res. C **95**, 11 531 (1990); W.B. Wright, R. Budakian, and S. J. Putterman Phys. Rev. Lett. **76**, 4528 (1996)
[9] M. Takeda and K. Mutoh, Appl. Opt. **22**, 3977 (1983)
[10] P. Cobelli *et al.*, Exp. Fluids **46**, 1037 (2009)
[11] E. Falcon, C. Laroche and S. Fauve, Phys. Rev. Lett. **98**, 094503 (2007)
[12] Y. V. Lvov, S. Nazarenko and B. Pokorni, Physica D **218**, 24 (2006)
[13] M. S. Longuet-Higgins, J. Fluid Mech. **16**, 138 (1963); A. V. Fedorov, W. K. Melville, and A. Rozenberg, Phys. Fluids **10**, 1315 (1998) and references therein.
[14] E. Falcon, S. G. Roux and C. Laroche, accepted in EPL (2010)
[15] P. Denissenko, S. Lukaschuk and S. Nazarenko, Phys. Rev. Lett. **99**, 014501 (2007)
[16] V. E. Zakharov and N. N. Filonenko, Sov. Phys. Dokl. **11**, 881 (1967)
[17] V. G. Polnikov, Wave Motion **33**, 271 (2001)

[18] Y. Choi, Y. V. Lvov, S. Nazarenko and B. Pokorni, Phys. Lett. A **339**, 361 (2005)